Article

Advancing Precise Orbit Determination and Precise Point Positioning of BDS-3 Satellites from B1IB3I to B1CB2a: Comparison and Analysis

Chen Wang [1,2,3], **Tengjie Luo** [1,2], **Shitong Chen** [1] **and Pan Li** [1,3,*]

1   College of Geological Engineering and Geomatics, Chang'an University, Xi'an 710054, China;
    chen.wang@chd.edu.cn (C.W.)
2   Big Data Center for Geosciences and Satellites, Chang'an University, Xi'an 710054, China
3   Key Laboratory of Western China's Mineral Resources and Geological Engineering, Ministry of Education,
    Xi'an 710054, China
*   Correspondence: lipan@chd.edu.cn

Abstract: The third generation of the Chinese BeiDou Navigation Satellite System (BDS-3) broadcasts new signals, i.e., B1C, B2a, and B2b, along with the legacy signals of BDS-2 B1I and B3I. The novel signals are demonstrated to show adequate upgraded performance, due to the restrictions on the ground tracking network for the BDS-3 satellites in new frequency bands, and in order to maintain the consistency of the hybrid BDS-2 and BDS-3 orbit/clock products using the common B1IB3I data, the use of B1CB2a observations is not sufficient for both precise orbit determination (POD) and precise point positioning (PPP) applications. In this study, one-year data of 2022 from the International GNSS Service (IGS) and the International GNSS Monitoring and Assessment System (iGMAS) are used in the precise orbit and clock determination for BDS-3 satellites based on the two sets of observations (i.e., B1IB3I and B1CB2a), and the orbit and clock accuracy along with the PPP ambiguity resolution (AR) performance are investigated. In general, the validations demonstrate that clear improvement can be achieved for the B1CB2a-based solution for both POD and PPP. In comparison to the B1IB3I, using BDS-3 B1CB2a observations can help to improve orbit consistency by around 25% as indicated by orbit boundary discontinuities (OBDs), and this use can further reduce the bias and enhance the orbit accuracy as revealed by satellite laser ranging (SLR) residuals. Similar improvement was also identified in the satellite clock performance. The B1CB2a-based solution obtains decreased Allan deviation (ADEV) values in comparison with the B1IB3I-based solution by 6~12%. Regarding the PPP-AR performance, the advantage of B1CB2a observations is evidently reflected through the estimates of wide-lane/narrow-lane fractional cycle bias (FCB), convergence time, and positioning accuracy, in which a significant reduction over 10 min is found in the PPP convergence time.

Keywords: BDS-3; precise orbit determination; precise point positioning; ambiguity resolution; B1C/B2a frequencies

1. Introduction

The Chinese BeiDou Navigation Satellite System (BDS), providing a global positioning, navigation, and timing (PNT) service, was officially announced to start commissioning at the end of July 2020. As 1 of the Big 4 Global Navigation Satellite Systems (GNSSs), BDS integrates navigation and communication functions and possesses multiple capacities [1,2]. Currently, the BDS hybrid constellation consists of both the second regional (BDS-2) and third global generation system (BDS-3) satellites. Compared to the BDS-2 system, the upgraded satellite buses, inter-satellite-links payloads, passive hydrogen masers (PHMs), and new signals with novel modulation techniques are utilized. It is worth noting that the BDS-3 satellites also broadcast the backward compatible BeiDou-2 B1I and B3I signals to ensure the smooth transition from BDS-2 to BDS-3.

In comparison to the old BDS-2 signals, the new B1C, B2a, and B2b signals in BDS-3 were anticipated to show a performance improvement both in the flexibility of signal modulation and diversified service. In particular, the B1C and B2a signals have been designed to meet the requirements of compatibility and interoperability with the L1 and L5 frequencies of GPS and Galileo [3]. As for the BDS-3 signal quality, the carrier-to-noise ratio (CNR) of the B2a signal is greater than that of the B1C, B1I, and B3I signals. Compared to other BDS-3 signals, the B2a signal has the most powerful anti-multipath capabilities, almost equivalent to the GPS L5. This was further identified by the GNSS receiver onboard the Haiyang-2D (HY-2D) China Ocean satellite [4]. In addition, the code and phase noises of the three new signals in BDS-3 were reported to be smaller than those of legacy signals at the same frequencies using zero-baseline experiments [5,6]. Moreover, the elevation-dependent satellite-induced code bias, which is identified by the multipath combination of BDS-2 satellite signals, was not obvious for all the signals of the BDS-3 satellites [7–9]. These studies provide a basis to further exploit the benefits of BDS-3 for precise orbit determination (POD) along with point precise positioning (PPP) using these new signals, especially with the B1C and B2a observations.

For POD of the BDS-3 satellites, several studies have analyzed the BDS-3 orbit performance using new frequencies of BDS-3 satellites and have reported that the BDS-3 satellites may benefit from a better ionosphere-free (IF) combination residual with the B1CB2a observations [10–12]. An average overlapping precision of 24.2 cm for BDS-3 satellites using 9 MGEX B1C/B2a measurements was presented in [13], while their results showed that the quality of B1CB2a-based orbits was improved by approximately 9% compared to the B1IB3I-based POD results. The advantage of the B1CB2a dual-frequency measurements was further indicated in [14], which increased the narrow-lane ambiguities fixing rate by nearly 8% compared to the B1IB3I-based orbits. The aforementioned studies suggested the prioritization of the B1CB2a signals, while a 72 h POD arc was generally used to reduce the limitation of the available ground observations. In addition, the orbit and clock products provided by the Analysis Centers (ACs) of the International GNSS Monitoring and Assessment System (iGMAS [15]) were assessed comprehensively by several studies, and their investigations indicated that improvements with regard to orbit and clock accuracy and stability for the B1CB2a-based solutions can be expected once the restrictions of the accessible ground tracking data on the BDS-3 new frequency bands are gradually mitigated [16,17]. The measurements from ground tracking networks increased rapidly after the beginning of 2021, especially for the new B1CB2a signals (see Figure 1). It provides a basis for generating reliable orbit and clock products for BDS-3 satellites.
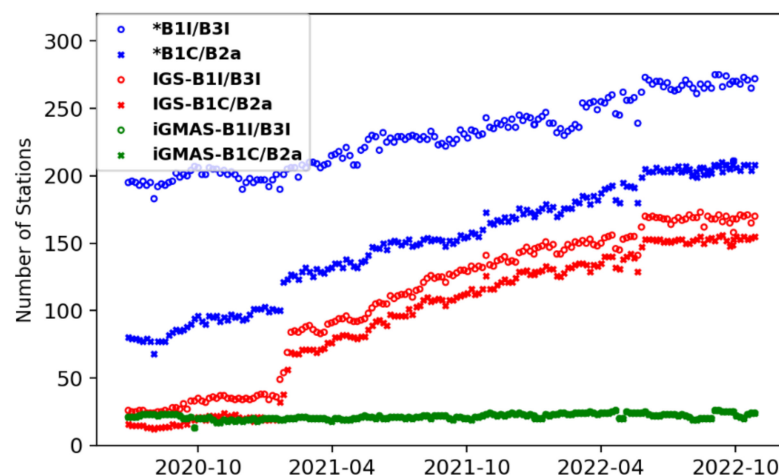

Figure 1. The number of ground stations tracking BDS-3 signals. (The cycles are stations with B1IB3I, and the cross represents the B1CB2a signal capacity. '*' illustrates the station tracking at least one BDS-3 satellite. The red and green marks represent IGS and iGMAS stations with full BDS-3-tracking capacity, respectively).

From the view of positioning, contributions were made with respect to performing and evaluating the basic positioning performance with the BDS-3 new signals. The preliminary PPP performance analysis of the BDS-3 satellites was reported in [18], and the results indicated that the accuracy of the standard point positioning based on the B2a was not comparable to that of the B1I signal. Later, study showed that the static PPP and kinematic PPP positioning errors of about 3 cm and 10 cm could be obtained when using the BDS-3 B1C and B2a signals [19]. More importantly, the multi-frequency signals bring new opportunities for ambiguity resolution (AR) of PPP, and the preliminary resolution of the fractional cycle bias (FCB) is presented, which would help to shorten the convergence time and improve accuracy [20–23]. For the phase bias estimation, the observable-specific signal biases (OSBs) were estimated for BDS-3 B1I/B3I/B1C/B2a, and the results indicated that B1C/B2a combination of BDS-3 can improve the single-epoch PPP accuracy, in addition to greatly shortening the convergence time compared to the results using the B1IB3I observations both in kinematic and static modes [24].

Although previous studies confirmed the priority of the new BDS-3 B1C and B2a signals, all the ACs across the International GNSS Service Multi-GNSS pilot project (IGS MGEX [25]), including the German Research Centre for Geosciences (GFZ), Center for Orbit Determination in Europe (CODE), Information and Analysis Center (IAC), Shanghai Astronomical Observatory (SHAO), and Wuhan University (WHU) [26–29], have been utilizing the observations of BDS-2 legacy B1I and B3I frequencies for their BDS-3 solutions since 2018, when the BDS-3 basic system started its open service. One reason for this is that the ground tracking network for the BDS-3 satellites was restricted, especially for the B1CB2a signals, as it would take a long period for the receiver firmware to upgrade after the Interface Control Document (ICD) was released. In addition, using the common B1I and B3I frequencies might help to retain the consistency of the BDS-2 and BDS-3 orbit and clock products.

In this study, the performance of the B1CB2a- and B1IB3I-based orbit and clock products with 24 h arc for BDS-3 satellites are compared and analyzed. The benefit of B1cB2a observations is presented not only for the determined orbit quality but also for the clock accuracy and stability. In addition, the impact of the two sets of the BDS-3 orbits on PPP-AR is also investigated.

Following the section on the overview of data collection and availability, the POD and PPP strategies are described in Section 3. Afterwards, the orbit boundary discontinuity (OBD) and satellite laser ranging (SLR) residuals are used as the metrics to evaluate the orbit quality, while the linear clock fit (LCF) and Allan deviation (ADEV) values are utilized to assess the accuracy and stability of the onboard atomic clock. Then, PPP-AR performance is investigated in terms of the FCB estimation, convergence time, and position accuracy. Finally, the findings of this study are discussed and conclusions are drawn in the final section.

2. Data Collection and Availability

The tracking data from the iGMAS and IGS ground tracking networks can be obtained and used for BDS-3 analysis [15,30]. For the stations of the iGMAS network, receivers (i.e., GMR-4011, GNSS_GGR, and UB4B0) from mainly three Chinese domestic manufacturers of the 20th and 54th Institute of China Electronics Technology Corporation along with Unicore Communication Ltd. were tested and upgraded to receive and decode B1I, B3I, B1C, and B2a signals since the BDS-3 experimental satellites were deployed in 2015. On the other hand, IGS has enabled a gradual increment in the number of receivers with BDS-3-tracking capability. Those ground stations equipped with Septentrio PolaRx5, Trimble NetR9, and JAVAD TRE-3 Delta receivers started to receive BDS-3 signals since the development of firmware 5.2.0, 5.37, and 3.7.3p1. Most of the IGS receivers can only track the B1I and B3I signals or single-frequency signals for BDS-3 satellites, while half of them cannot support the reception of the new BDS-3 B1C and B2a signals as shown in Figure 1. In addition, not all the satellites in the BDS-3 constellation were tracked by those receivers. For some

receivers, the BDS-3 satellite with Pseudo Random Noise (PRN) number beyond C37 cannot be recorded. Fortunately, the situation improved when the receivers were upgraded with accelerated firmware in the beginning of 2021 (See Figure 1). In early 2022, the total number of globally distributed tracking stations with full BDS-3 constellation tracking capacity reached around 150. This could ensure a reliable and sufficient data source in BDS-3 satellites' analysis. Hence, we chose the whole year of 2022 as our test period for POD and PPP performance evaluation and investigation, and about 110 ground stations from IGS and iGMAS were selected in this study. All of these stations are capable of tracking the whole BDS-3 constellation at all frequencies to ensure an equivalent POD condition in terms of the observations using B1IB3I and B1CB2a, respectively. The ground network distributions are depicted in Figure 2.
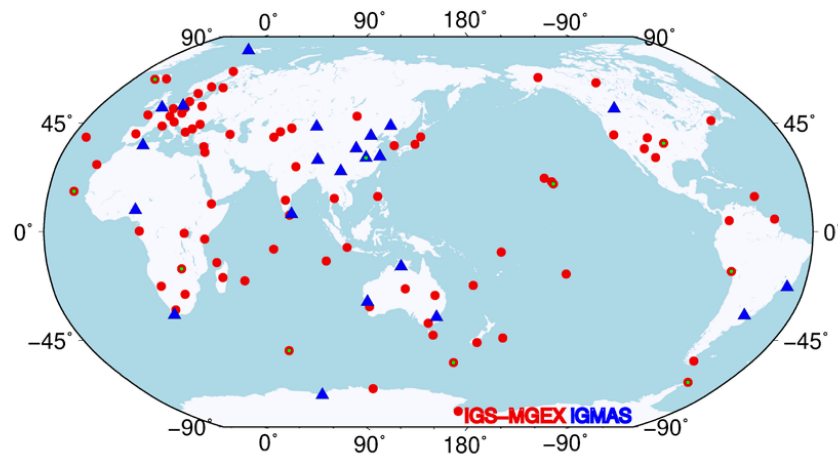

Figure 2. The ground tracking stations from IGS and iGMAS for BDS-3 satellites (10 stations marked with green points are used for PPP experiment).

As mentioned above, there are four BDS-3 open service signals (i.e., B1I, B3I, B1C, and B2a) transmitted by BDS-3 satellites, which yield two types of dual-frequency ionosphere-free (IF) combinations from the legacy and new signals (i.e., B1IB3I and B1CB2a), respectively. For phase and code, the basic IF observations can be represented as follows:

$$PC = n_1\phi_1 + n_2\phi_2$$
$$LC = n_1P_1 + n_2P_2 \tag{1}$$

where

$$n_1 = \frac{f_1^2}{f_1^2 - f_2^2}; \quad n_2 = -\frac{f_2^2}{f_1^2 - f_2^2} \tag{2}$$

Although the dual-frequency IF combination eliminates the effects of first-order ionospheric delays, it in turn amplifies the observation noise. By simply assuming the same observation error (σ) for both input frequencies, the IF observation errors (σ_{IF}) for the code or phase can be derived as follows:

$$\sigma_{IF} = \sqrt{n_1^2 + n_2^2}\sigma \tag{3}$$

Inputting the frequency values of B1I (1561.078 MHz), B3I (1367.52 MHz), B1C (1575.42 MHz), and B2a (1176.45 MHz) into Equation (3), one can obtain the noise factors for dual-frequency IF combination of B1IB3I and B1CB2a, which are 3.79 and 2.82, respectively. This factor can multiply the observation noise along with effects that are not fully absorbed by observation models and accordingly influence the performance of POD or of PPP.

For the BDS-3 constellation, the Shanghai Engineering Center for Microsatellites (SECM) of the China Academy of Science (CAS) manufactured ten BDS-3 MEO satellites,

while the remaining 14 out of the 24 BDS-3 MEO satellites were manufactured by the China Academy of Space Technology (CAST). In addition, all of the BDS-3′s Geostationary Earth Orbit (GEO) and IGSO satellites were designed and created by CAST, which is the only satellite vehicle provider for the BDS-2 GEO, IGSO, and MEO satellites. As the BDS-3 GEO satellites only broadcast signals to B1I and B3I, to keep the consistency of the comparison between B1I/B3I and B1C/B2a POD and PPP, the analysis to BDS-3 GEOs are not included in this study.

3. POD and PPP Strategies

This section focuses on describing and presenting the data processing strategies for BDS-3 POD and PPP with ambiguity resolution.

3.1. POD Strategies

A two-step POD solution is used for the POD in this study as illustrated in [31]. In the first step, precise orbit and clock products from WUM (Wuhan University MGEX AC) are used to estimate the ground station coordinates, corresponding receiver clocks, and the troposphere zenith delays. Then, in the second step, these estimated parameters are fixed. It should be noted that there are two different yaw attitude mechanisms used by the BDS-3 satellites manufactured by CAST and SECM. We have incorporated them into the modified version of Position And Navigation Data Analyst (PANDA) software [32]. It is worth noting that an empirical constant acceleration in the along-track direction is also introduced as in [31]. The code observation quality differs in each frequency for different measurements, while the POD performance is hardly affected as the code measurement is assigned a lower weight by a factor of 100 compared to the phase measurement. In addition, one should note that the signal-specific phase center offsets (PCOs) for BDS-3 satellites officially released by the China Satellite Navigation Office (CSNO) are used in this study. Table 1 lists the summary of the POD models and processing parameters used in this study. In particular, the a priori box-wing model was adopted to enhance the five-parameter ECOM [33], and the Earth radiation model was applied in the visible spectrum [34]. The B1CB2a- and B1IB3I-based PODs are performed using the same strategies except for the observations that are used.

Table 1. Summary of the models and strategies applied.

Models	Descriptions
Observations	Ionosphere-free observations of B1IB3I and B1CB2a
Time period	DOY 1 to 365 in 2022
Arc length and interval	24 h and 30 s
Elevation angle cutoff	10 degrees
Observation weight	Elevation > 30°: 1; Elevation ≤ 30°: $2 \times \sin(e)$
BDS-3 PCO values	Values from CSNO [35]
Tropospheric delay	Saastamoinen model for a priori dry and wet zenith delay model with estimation of wet delay global mapping function for dry and wet zenith delays [36]
Gravity model	EGM2008 with 12 degrees and orders
Third body effect	Applied
Satellite attitude model	Continuous yaw steering models [37,38]
Solar radiation pressure	5-parameter ECOM with a priori box-wing model [33]
Relativistic effects	IERS conventions 2010 [39]
Solid earth pole tides	IERS conventions 2010 [39]
Ocean tides	None
Earth radiation model	Applied [34]
Antenna thrust	Applied [40]
Ambiguity fixing	Fixed to integer [41]
Inter system bias (ISB)	Estimated as arc-dependent constant for each receiver
Parameters estimated	Orbit dynamic parameters, initial satellite positions and velocities, ISB, ambiguity, etc.

3.2. PPP Strategies

For PPP, we designed three schemes to evaluate the performance as listed in Table 2. The first two schemes were performed when two types of IF observations were used consistently with the orbit and clock products. Scheme 3 investigates the cases when the B1CB2a combination is employed in PPP when the related orbit and clock products were not available, which is validated by the fact that the BDS-3 orbit and clock products determined with new signals are currently not promoted in the IGS community. For ambiguity resolution, the method proposed by Ge et al. [42] was adopted. Firstly, in the server side, the satellite FCB products of wide-lane and narrow-lane are estimated by utilizing the average of fractional parts of all pertinent wide-lane and narrow-lane ambiguity estimates derived from the Melbourne–Wübbena and ionosphere-free combination measurements, respectively. In the user side, the wide-lane and narrow-lane FCBs are applied to the corresponding ambiguities in order to remove the satellite hardware delay [20,22]. For determining receiver biases, the single-difference-between-satellite operation is performed by selecting a reference satellite. The integer resolution strategy is applied to the wide-lane first, and then to the narrow-lane ambiguities after the successful resolution of wide-lane ambiguities. Once the wide-lane and narrow-lane ambiguities have been fixed, the least-squares ambiguity decorrelation adjustment (LAMBDA [43]) approach is used for ambiguity research. For ambiguity validation, first, we use the round-off criterion of 0.25 cycle for the fractional part check of WL and NL ambiguities. Then, the ratio test was used for ambiguity validation to search the best NL integer solution with the threshold of 3.0.

Table 2. PPP-AR solutions using different types of observations and orbit products.

	Observations for POD	Observations for PPP
Scheme 1	B1IB3I	B1IB3I
Scheme 2	B1CB2a	B1CB2a
Scheme 3	B1IB3I	B1CB2a

Three signal selection schemes are abbreviated as "S1", "S2", and "S3", and for PPP experiments, "-Flo"/"-AR" is added to the abbreviations to distinguish the ambiguity-float and ambiguity-fixed solutions. In total, six groups of PPP solutions are calculated.

4. Analysis and Comparison of Results

The results for products of orbit and clock are compared based on validation metrics in this section. We also evaluate the positioning performance including the estimation of the wide-lane/narrow-lane FCB, convergence time, and position error.

4.1. Orbit Performance

The orbit quality can be evaluated using the internal and external metrics. As an internal validation indicator of orbit quality, the orbit boundary discontinuity (OBD) was used to assess the orbit accuracy, in which two POD arc position differences at the midnight epoch were calculated. The OBDs were treated as outliers and removed once the three-dimensional (3D) values of the orbit differences were larger than 100 cm. On the other hand, satellite laser ranging (SLR) is an independent and common tool for external orbit evaluation in terms of orbit accuracy and precision, especially in the radial direction. The SLR residuals are of the so-called OMC (observation minus computed) type. The residual is treated as gross error once it is over 20 cm.

Figure 3 shows the mean OBD values in the along-track, cross-track, and radial directions for the two sets of POD solutions determined with B1IB3I and B1CB2a observations, and Table 3 summarizes these mean values. In general, the orbits generated from the new B1CB2a observations clearly show lower OBDs compared to that from the legacy B1IB3I signals for all the BDS-3 IGSO and MEO satellites. This can be attributed to the lower IF observation noise factor of new B1CB2a signals, which produce a reduction of approxi-

mately 25% compared to the old IF combination as calculated by Equation (3). In addition, quite similar orbit performance can be found for the two types of MEOs manufactured by CAST and SECM. While the IGSO satellites display worse OBD values by one order of magnitude, especially in the orbit radial direction. This is probably caused by the smaller nadir angle caused by the higher orbit altitude of IGSOs compared to the MEOs, which makes the orbit parameters much harder to separate from the other estimated parameters. In addition, the large communication antenna deployed on the BDS-3 IGSO may also result in orbit dynamic modeling issues [9], and these issues may need further investigation.
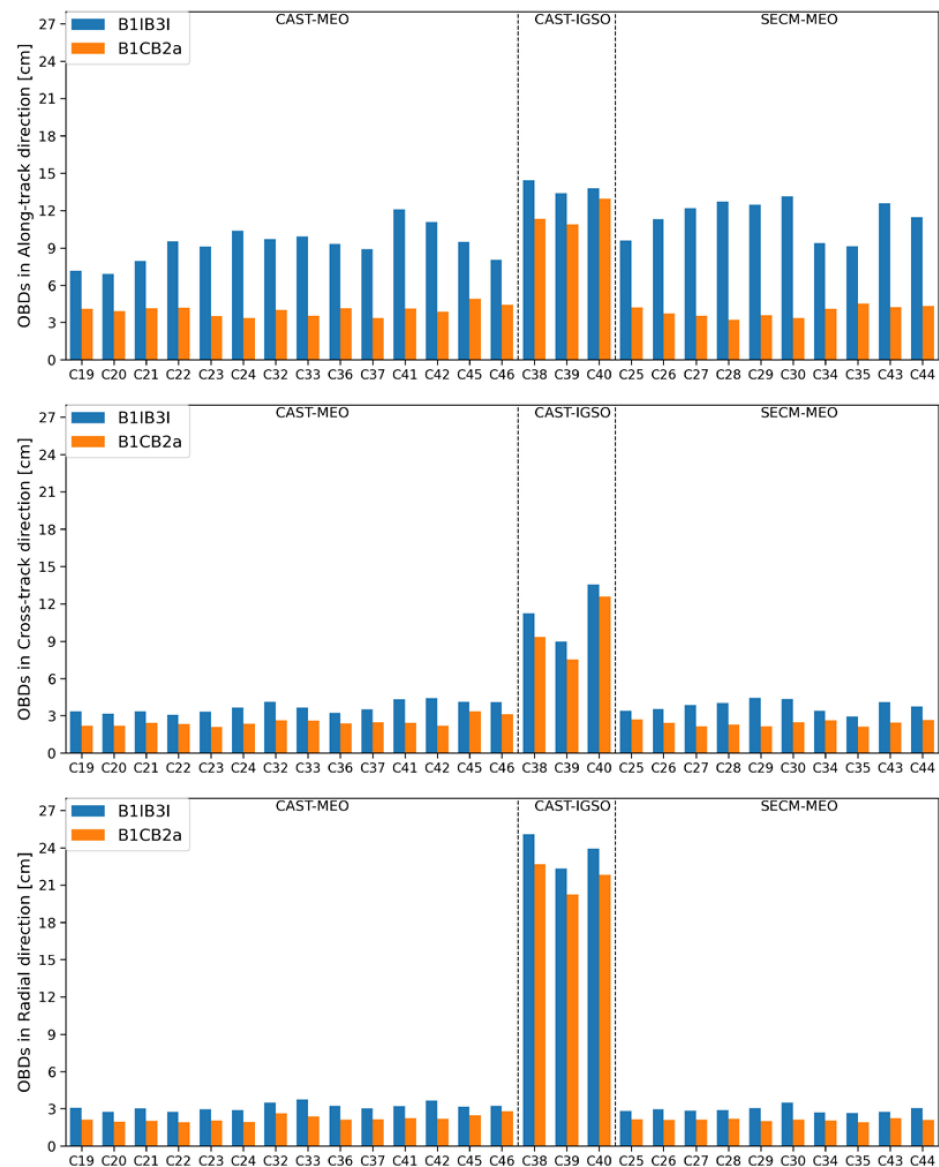

Figure 3. OBDs for solutions using B1IB3I and B1CB2a in radial, cross-track, and along-track directions.

Table 3. Mean value of OBDs in along-track, cross-track, and radial directions for BDS-3 B1IB3I and B1CB2a solutions (unit: cm).

Solution	Along-Track			Cross-Track			Radial		
	CAST-MEO	CAST-IGSO	SECM-MEO	CAST-MEO	CAST-IGSO	SECM-MEO	CAST-MEO	CAST-IGSO	SECM-MEO
B1IB3I	9.2	13.9	11.4	3.7	11.2	3.8	3.2	23.1	2.9
B1CB2a	4.0	11.7	3.9	2.5	9.8	2.4	2.2	20.6	2.1

Figure 4 depicts the time series of the SLR residuals for the two types of solutions. During the test period, there were only four BDS-3 satellites, i.e., C20(M2) and C21(M3) from CAST and C29(M9) and C30(M10) from SECM, tracked by the International Laser Ranging Service (ILRS). As can be seen, the B1CB2a-based solution demonstrates a reduction in the mean SLR residuals, where a shift around 0.7 cm and 1.1 cm can be obtained for CAST and SECM satellites, respectively. The mean value of the SLR residuals indicates the accuracy between the calculated orbit and the reference orbit. In addition, the standard deviation (STD) of SLR residuals is an indicator to demonstrate the orbit precision. It can be seen that the B1CB2a-based solutions show slightly improved accuracy compared to the B1IB3I by about 0.3 cm. It is worth noting that the mean values of the SLR residuals of B1IB3I and B1CB2a have opposite signs for the two SECM satellites, i.e., C29 and C30. This may be attributed to modeling issues related to the Earth albedo and antenna thrust [30]. However, for all the four BDS-3 satellites, a common phenomenon is observed when the observations are switched from B1IB3I to B1CB2a, i.e., a notable shift of up to 1 cm in SLR residuals. In general, the benefit of B1CB2a observations in both shifting the systematic bias in the radial direction and improving the orbit precision is further confirmed with SLR validations.
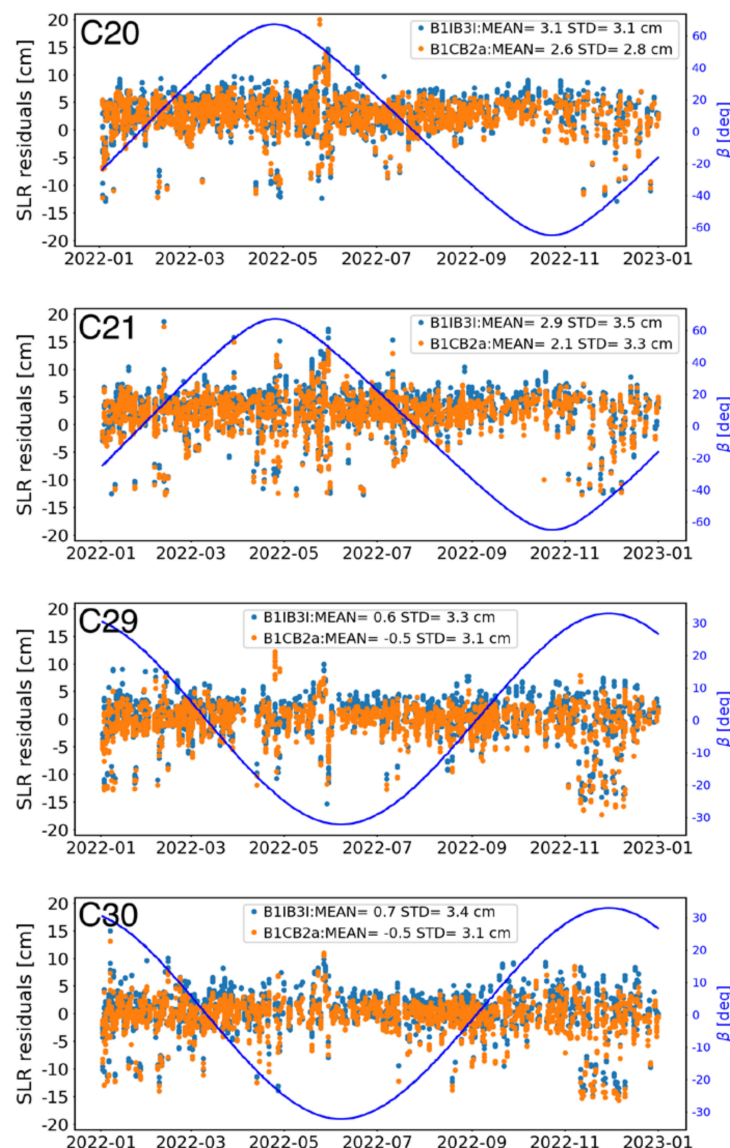

Figure 4. SLR residuals of four BDS-3 satellites, i.e., C20 and C21 of CAST and C29 and C30 of SECM, for the two solutions using B1IB3I and B1CB2a observations. The blue lines represent the elevation angle over orbital plane.

4.2. Clock Performance

The BDS-3 MEO and IGSO satellites are each equipped with four atomic clocks on-board. For CAST MEO satellites, the Rubidium atomic frequency standard (RAFS) clock is generally used as the primary standard, whereas for IGSOs and the other two MEO satellites, the passive hydrogen maser (PHM) clock is used as the primary frequency standard. For SECM MEO satellites, two Chinese PHM clocks are used as primary frequency standards, while two RAFS clocks are used as prospective backup. The onboard primary clock types are summarized in Table 4. For clock quality analysis, the linear clock fit (LCF) and the overlapping Allan deviation (ADEV) are computed for clock performance assessment.

The LCF accounts for the residuals after removing the linear fit of the epoch-wise clock for each day, which is commonly used to evaluate the clock performance. It is worth noting that the orbit errors are highly coupled with the clock estimates; hence the LCF value indicates not only the clock quality but also the partial absorption of the orbit error, especially in the orbit radial direction. Figure 5 is a plot of the root mean square (RMS) values of the LCFs for all BDS-3 MEO and IGSO satellites during the test period. Similar to the results of OBDs, the clock solution also confirms the prioritization of using the B1CB2a observations. The overall mean RMS values of B1IB3I and B1CB2a LCFs are about 0.21 ns and 0.19 ns, respectively. This means that B1CB2a clocks are improved by approximately 9% compared to the B1IB3I clocks in terms of their LCFs. In addition, it is observed that the LCFs of the CAST MEOs are larger than those of the SECM MEOs. These noticeable LCF differences can be attributed to the behavior between the onboard RAFSs and PHMs. Notably, the three CAST IGSOs are also equipped with the PHMs for their primary clocks; furthermore, they achieve the highest LCFs, on average, among the three types of satellites. These higher values probably result from the relatively larger orbit errors of the IGSOs due to their smaller nadir angle compared to the MEOs, and also, LCFs can partly absorb the orbit errors, mainly in the radial direction.
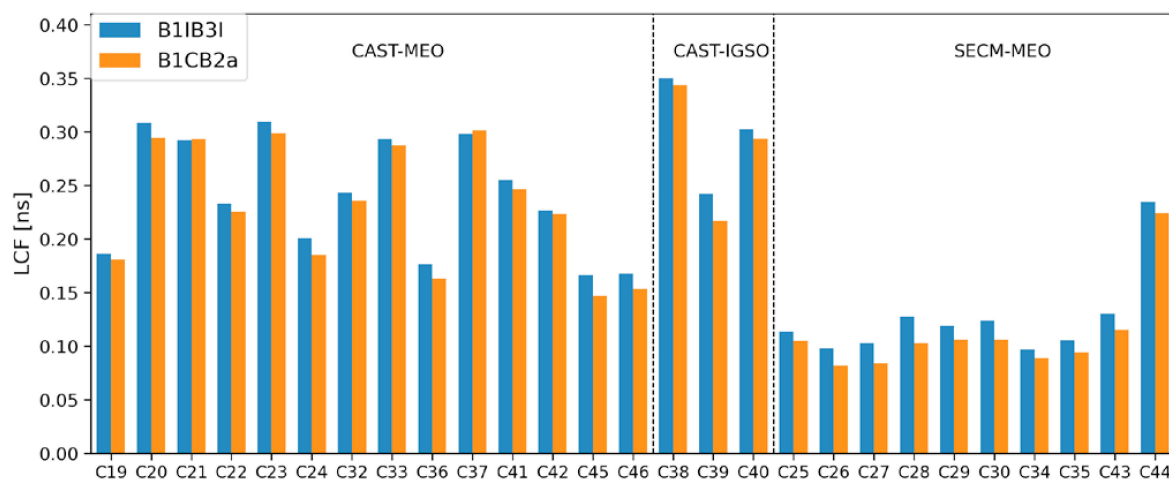

Figure 5. LCFs of solutions using B1IB3I and B1CB2a observations.

The clock quality could also affect the assessment of the clock stability. In order to assess the performance of the BDS-3 onboard clocks, ADEVs computed for GPS week 2243 (2–8 January 2022) using the 30 s clock estimates are shown in Figure 6, and Table 4 summarizes the clock frequency stability for the two sets of solutions. In general, the B1CB2a solution obtains slightly smaller ADEVs compared to the B1IB3I solution, i.e., by 6~12%; however, the two solutions display a similar pattern. In particular, a visible bump appears at the integration time of 10,000 s. This may be attributed to the orbit modeling deficiencies that occur at roughly half of the orbital period in the ADEVs, and these deficiencies may need further investigation. In addition, a subsequent increase in the ADEV values is observed for all three IGSOs, while the performance of the BDS-3 clocks is comparable to that in the results of [27].
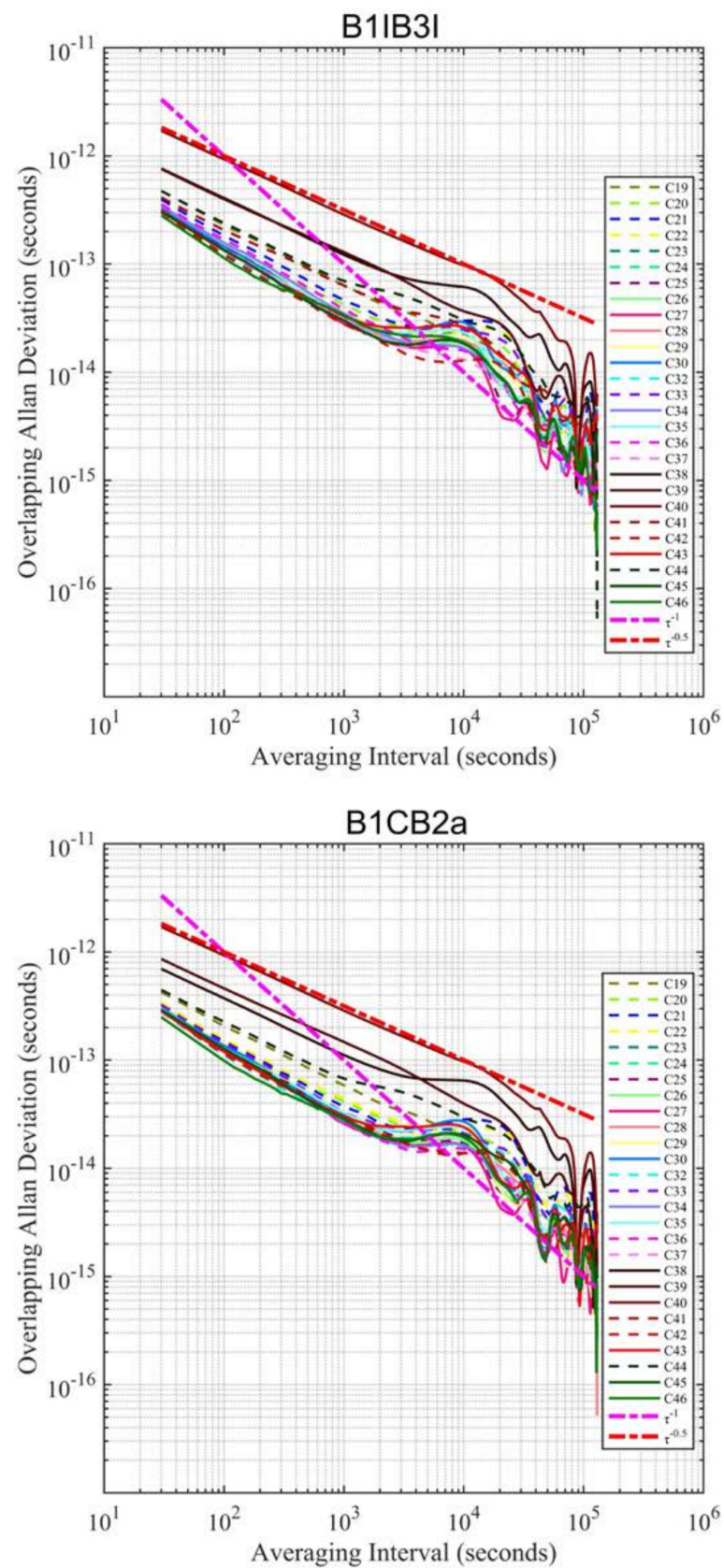
Figure 6. ADEVs for the two clock solutions using B1IB3I (**upper panel**) and B1CB2a (**bottom panel**).

Table 4. Clock frequency stability of BD3 MEO and IGSO satellites.

PRN		Primary Clock Type	1000 s ($\times 10^{-14}$)		10,000 s ($\times 10^{-14}$)	
			B1I/B3I	B1c/B2a	B1I/B3I	B1c/B2a
MEO-CAST	C19	Rb	6.06	5.66	2.20	1.93
	C20	Rb	4.23	4.10	2.20	2.13
	C21	Rb	4.35	3.45	2.98	2.84
	C22	Rb	3.54	4.32	2.40	2.33
	C23	Rb	3.41	3.12	2.18	1.71
	C24	Rb	3.21	2.71	1.86	1.58
	C32	Rb	2.92	2.84	1.93	2.03
	C33	Rb	3.05	3.04	2.55	2.11
	C36	Rb	3.60	2.56	1.53	1.45
	C37	Rb	2.96	2.99	1.30	1.39
	C41	Rb	6.39	2.83	2.65	1.36
	C42	Rb	2.71	3.06	1.28	1.38
	C45	PHM	2.70	2.59	1.84	2.01
	C46	PHM	3.59	2.85	1.92	1.92
MEO-SECM	C25	PHM	3.18	2.89	1.95	1.67
	C26	PHM	3.12	3.06	1.81	1.83
	C27	PHM	2.65	2.43	1.66	1.61
	C28	PHM	2.86	2.58	1.88	1.87
	C29	PHM	3.26	3.12	2.14	2.01
	C30	PHM	3.23	2.99	2.89	2.70
	C34	PHM	3.33	2.56	1.73	1.63
	C35	PHM	3.27	3.15	2.37	2.33
	C43	PHM	3.24	2.92	2.60	2.40
	C44	PHM	7.47	6.76	3.04	2.93
IGSO-CAST	C38	PHM	11.80	10.80	6.16	6.19
	C39	PHM	13.10	12.00	3.68	3.58
	C40	PHM	28.90	28.90	9.80	9.77

4.3. FCB Performance

High-quality FCB correction is the key to reliable PPP ambiguity resolution. For FCB estimation, the same signals that are consistent with the PPP processing should be used. We estimate the FCB for each signal selection scheme, and their qualities in terms of wide-lane and narrow-lane site usages are shown in Figure 7. The wide-lane ambiguity is obtained with the MW observation linear combination and is not related to the precise satellite orbit and clock.

It is observed that S2 and S3 have nearly the same wide-lane ambiguity usage because both of their wide-lane ambiguities are calculated using the B1CB2a dual-frequency code and phase observations. Their usage ranges from 98.7% to 99.5%. The S1 wide-lane usage is lower than that of S2 and S3 and ranges from 96.0% to 97.4%. The wide-lane usage comparison also demonstrates that B1CB2a has better signal quality than B1IB3I. Different from the wide-lane ambiguity, the narrow-lane ambiguity estimation is related to both the raw dual-frequency observation and the precise satellite orbit and clock. Hence, the usage of narrow-lane ambiguities is simultaneously influenced by these two factors. The narrow-lane usage ranges from 96.7% to 98.1%, 98.5% to 99.1%, and 97.6% to 98.7% for S1, S2, and S3, respectively. As indicated in POD and precise clock estimation analysis sections, the B1CB2a satellite orbit and clock precision is also better than the one of B1IB3I. Therefore, the S2 scheme achieves the highest usage while the S1 scheme achieves lowest. The S3 scheme uses the better B1CB2a observation but the worse B1IB3I precise products, leading to it being second best in terms of narrow-lane usage.
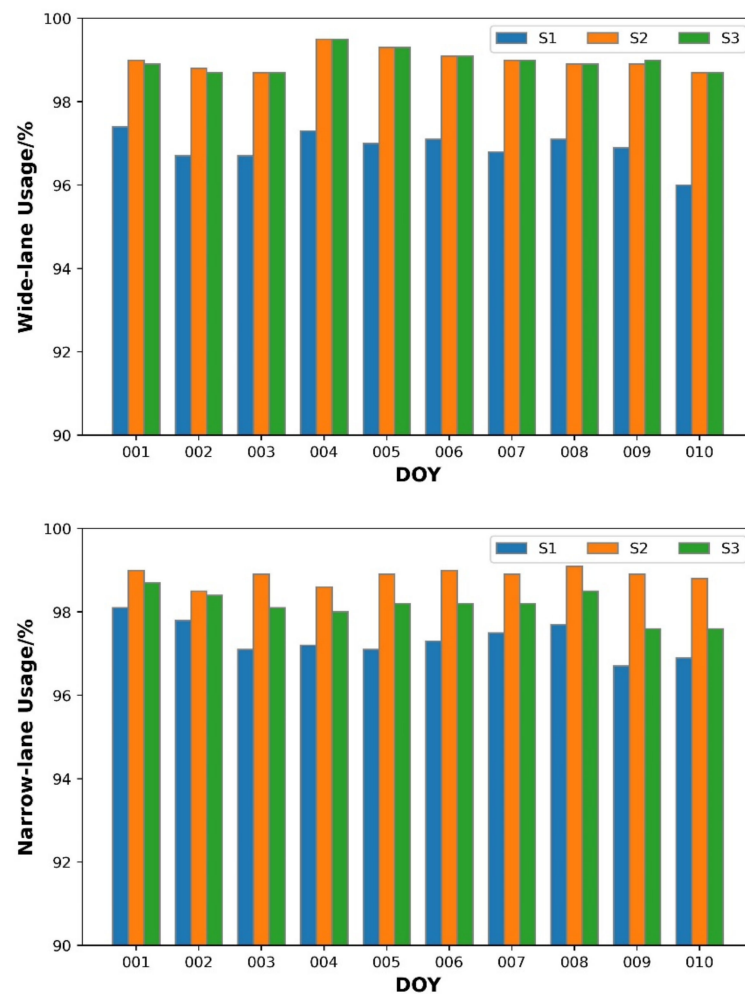
Figure 7. Wide-lane (**upper panel**) and narrow-lane (**bottom panel**) site usages using the three schemes.

4.4. PPP Performance

We selected the data from 10 MGEX stations during DOY 001-010 in 2022 for PPP experiments. Both ambiguity-float and -fixed BDS kinematic PPP solutions are performed with three signal selection strategies for comparison purposes. In these six solutions, the same pre-processing, error correction models and quality control methods are used. For PPP-AR, the same ambiguity-fixing strategies are utilized except that different FCB corrections are used.

The time series of the 68th percentile of the east, north, and vertical errors for all test samples is shown in Figure 8. First, we can observe that for each scheme, the positioning error time series of ambiguity-float and ambiguity-fixed solutions are close to each other, especially in the beginning period. The convergence time of the ambiguity-fixed solution is slightly shorter than that of the ambiguity-float solution. It is because the ambiguity needs a period, i.e., the time to first fix, to converge and be fixed. However, the three schemes clearly differ from each other in the first 1 h. It shows that the signal selection has a significant impact on the BDS's short-term PPP positioning, when compared to ambiguity fixing. Benefiting from the higher signal quality of the B1CB2a combination, in terms of anti-multipath and observation noise, B1CB2a S2 solution has the shortest convergence time and the highest positioning precision. The traditional B1IB3I S1 scheme ranks second. In S3, the inconsistent signal selection in POD + precise clock estimation on the service side and PPP on the user side may result in an error that causes modelling difficulties. Therefore, the PPP positioning error of S3 is much larger than that of S1 and S2. Comparing the results

of different components, we can also find that with a long observation span (about 80 min), six groups of positioning error lines almost coincide in the north and vertical directions while still having obvious differences in the east direction. The signal selection strategy has a greater impact on the east positioning precision with about two-hour observation data.
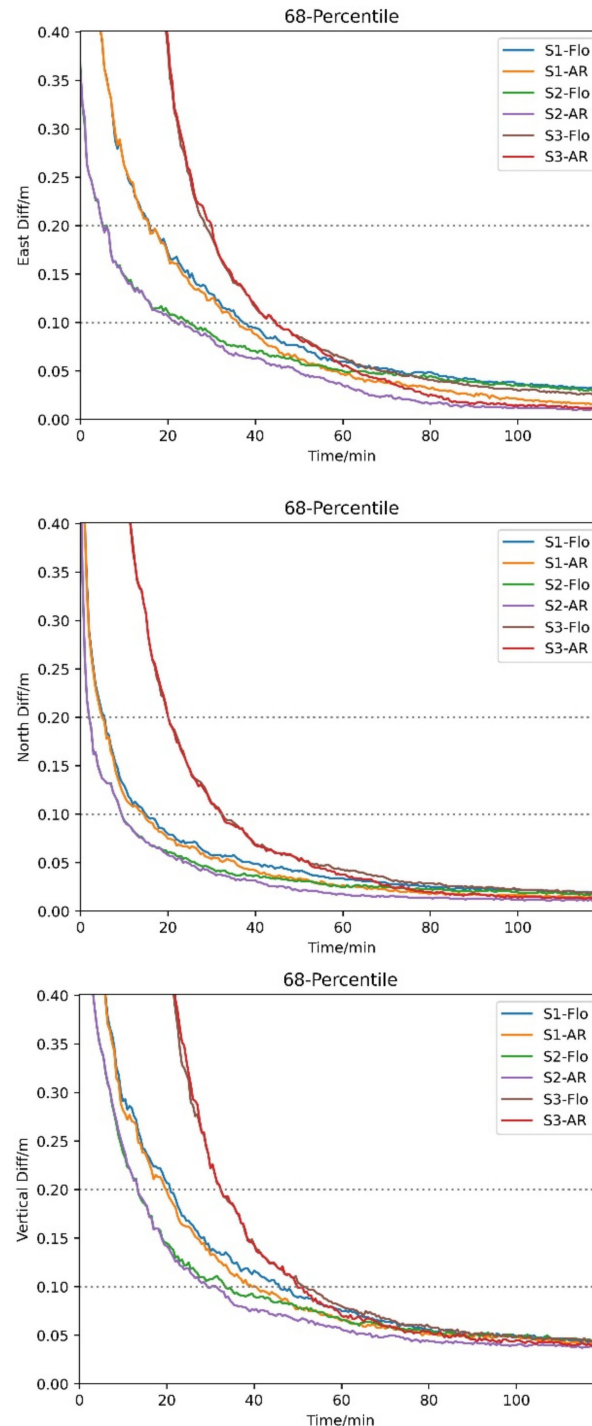

Figure 8. Time series of positioning errors of six PPP solutions (68% percentile) in East (**upper panel**), North (**middle panel**), and Up (**bottom panel**) components.

In this study, we define the time required for obtaining the positioning error of less than 1 dm over 10 consecutive epochs as the convergence time. The convergence time of the 68th percentile of BDS PPP solution in three directions is provided in Table 5. For all six solutions, the north direction has the fastest convergence while the vertical has the

slowest. PPP-AR slightly shortens the convergence time by 0 to 4 min. Among the three PPP-AR solutions, the S1-AR takes 36.5, 15.0, and 42.0 min to converge in the east, north, and vertical directions, respectively. Using the new B1CB2a signal combination, S2-AR significantly reduces the convergence time to 24.0, 9.5, and 30.5 min, with an improvement percentage of 34.2%, 36.7%, and 27.4% in the three directions, respectively.

Table 5. Convergence time of six PPP solutions (68% percentile).

PPP Result		East (min)	North (min)	Up (min)
S1	float	37.5	15.5	46.0
	AR	36.5	15.0	41.0
S2	float	25.0	9.5	33.5
	AR	24.0	9.5	30.5
S3	float	45.0	33.0	52.0
	AR	45.0	32.5	50.0

5. Discussion

Although previous studies demonstrated the improved performance of the new BDS-3 signals, the BDS-2 legacy B1IB3I observations are generally utilized, firstly, due to the limited B1CB2a data availability before 2021, and secondly, to maintain the consistency of products of the hybrid BDS-2 and BDS-3 within the common frequencies. Due to the limited accessibility of the B1CB2a-based orbit and clock products from IGS MGEX ACs, the PPP performance along with the PPP-AR associated with the new BDS-3 signals were not further investigated.

With the increasing number of ground tracking networks for BDS-3 satellites, a reliable and promising POD and PPP performance can be obtained with B1CB2a rather than with the B1IB3I observations. However, the lower accuracy of the BDS-3 IGSOs was observed due to the higher orbit altitude, which makes the orbit dynamic parameters much harder to separate from the other estimated parameters. The OBDs results also show that the BDS-3 MEOs could obtain an average of approximately 2 cm in radial direction of an orbit when using the B1CB2a observation. In addition, a visible bump appears at the integration time of 10,000 s. It may be caused by the orbit modeling deficiencies that occur at roughly half of the orbital period, and these deficiencies may need further investigation.

The inclusion of non-gravitational forces including the Earth albedo and antenna thrust decreases the movement of the satellites in the radial direction, and in turn increases the mean value (bias) of the SLR residuals. In this study, a gross optical parameter from CSNO metadata was used to calculate the Earth albedo in the visible light spectrum, while the calculation in the infrared spectrum was omitted. This is probably attributed to an erroneous bias as revealed by the SLR residuals. Similar to the Earth albedo, the antenna thrust force was calculated with parameters obtained from a previous experiment [39]. To be specific, the B1CB2a-based solution demonstrates a reduction in the mean SLR residuals, where a shift around 0.7 cm and 1.1 cm is obtained for CAST and SECM satellites, respectively. The mean value of the SLR residuals of B1IB3I and B1CB2a have opposite signs for the two SECM satellites, i.e., C29 and C30. This may be attributed to modeling issues related to the Earth albedo and antenna thrust. A common phenomenon is observed for all the four BDS-3 satellites when the observations switch from B1IB3I to B1CB2a, i.e., a notable shift of up to 1 cm in SLR residuals.

Further investigation of the modeling issues, in particular of the BDS-3 IGSOs and PPP-AR with multifrequency observations, should be conducted. In addition, the availability of the B1CB2a-based orbit and clock solutions is an urgent need, and an integrity convention for BDS-3 B1CB2a products can also be formulated as only B1IB3I signals are broadcasted by BDS-3 GEO satellites.

6. Conclusions

In this contribution, one-year data from IGS and iGMAS were used for orbit and clock determination of BDS-3 satellites based on the B1IB3I and B1CB2a observations, and then, the orbit and clock performance along with the PPP-AR performance were investigated with the two sets of POD daily solutions.

1. Regarding orbit quality, when compared with the orbits determined using B1IB3I observations, clear improvement in quality is achieved with the B1CB2a solution. The orbit consistency indicated by OBDs is improved by around 25% on average.
2. The SLR validations of the four BDS-3 MEOs indicate that the B1CB2a-based solution demonstrates a shift in the mean SLR residuals of around 1 cm, in addition to a slightly improved accuracy compared to that of the B1IB3I, by about 0.3 cm.
3. The B1CB2a solution obtains slightly smaller ADEVs in comparison with the B1IB3I solution, by 6~12%.
4. Regarding the PPP-AR performance, the advantage of the B1CB2a-based solution can be also observed with respect to the estimates of wide-lane/narrow-lane FCBs, convergence time, and positioning accuracy.
5. A significant reduction beyond 10 min in PPP convergence time was noted when the new BDS-3 signals were used. However, the worst PPP performance in convergence time and positioning accuracy was achieved if the observations and orbit/clock products were used inconsistently.

References

1. Yang, Y.; Mao, Y.; Sun, B. Basic performance and future developments of BeiDou global navigation satellite system. *Satell. Navig.* **2020**, *1*, 1. [CrossRef]
2. Montenbruck, O.; Steigenberger, P.; Hauschild, A. Comparing the 'Big 4'—A User's View on GNSS Performance. In Proceedings of the 2020 IEEE/ION Position, Location and Navigation Symposium (PLANS), Portland, OR, USA, 20–23 April 2020; pp. 407–418.
3. Lu, M.; Li, W.; Yao, Z.; Cui, X. Overview of BDS III new signals. *Navigation* **2019**, *66*, 19–35. [CrossRef]
4. Li, M.; Mu, R.; Jiang, K.; Wang, Y.; Zhang, X.; Chang, C.; Zhao, Q. Precise orbit determination for the Haiyang-2D satellite using new onboard BDS-3 B1C/B2a signal measurements. *GPS Solut.* **2022**, *26*, 137. [CrossRef]
5. Hou, P.; Zhang, B.; Yuan, Y.; Zhang, X.; Zha, J. Stochastic modeling of BDS2/3 observations with application to RTD/RTK positioning. *Meas. Sci. Technol.* **2019**, *30*, 095002. [CrossRef]
6. Chen, J.P.; Hu, X.G.; Tang, C.P.; Zhou, S.S.; Yang, Y.F.; Pan, J.Y.; Ren, H.; Ma, Y.X.; Tian, Q.N.; Wu, B.; et al. SIS accuracy and service performance of the BDS-3 basic system. *Sci. China Phys. Mech. Astron.* **2020**, *63*, 269511. [CrossRef]
7. Zhang, X.; Wu, M.; Liu, W.; Li, X.; Yu, S.; Lu, C.; Wickert, J. Initial assessment of the COMPASS/BeiDou-3: New-generation navigation signals. *J. Geod.* **2017**, *91*, 1225–1240. [CrossRef]

8. Zhou, R.; Hu, Z.; Zhao, Q.; Li, P.; Wang, W.; He, C.; Cai, C.; Pan, Z. Elevation-dependent pseudorange variation characteristics analysis for the new-generation BeiDou satellite navigation system. *GPS Solut.* **2018**, *22*, 60. [CrossRef]

9. Zhao, Q.; Guo, J.; Wang, C.; Lyu, Y.; Xu, X.; Yang, C.; Li, J. Precise orbit determination for BDS satellites. *Satell. Navig.* **2022**, *3*, 2. [CrossRef]

10. Xu, X.; Wang, X.; Liu, J.; Zhao, Q. Characteristics of BD3 global service satellites: POD, open service signal and atomic clock performance. *Remote Sens.* **2019**, *11*, 1559. [CrossRef]

11. Tan, B.; Ai, Q.; Yuan, Y. Analysis of Precise Orbit Determination of BDS-3 MEO and IGSO Satellites Based on Several Dual-Frequency Measurement Combinations. *Remote Sens.* **2022**, *14*, 6030. [CrossRef]

12. Mi, X.; Sheng, C.; EI-Mowafy, A.; Zhang, B. Characteristics of receiver-related biases between BDS-3 and BDS-2 for five frequencies including inter–system biases, differential code biases, and differential phase biases. *GPS Solut.* **2021**, *25*, 113. [CrossRef]

13. Li, R.; Wang, N.; Li, Z.; Zhang, Y.; Wang, Z.; Ma, H. Precise orbit determination of BDS-3 satellites using B1C and B2a dual-frequency measurements. *GPS Solut.* **2021**, *25*, 95. [CrossRef]

14. He, L.; He, X.; Huang, Y. Enhanced precise orbit determination of bds-3 meo satellites based on ambiguity resolution with b1c/b2a dual-frequency combination. *Measurement* **2022**, *205*, 112197. [CrossRef]

15. Jiao, W.; Ding, Q.; Li, J.; Lu, X.; Feng, L.; Ma, J.; Chen, G. Monitoring and assessment of GNSS open services. *J. Navig.* **2011**, *64*, S19–S29. [CrossRef]

16. Ye, F.; Yuan, Y.; Yang, Z. Validation and evaluation on B1IB3I-based and B1CB2a-based BDS-3 precise orbits from iGMAS. *Adv. Space Res.* **2022**, *70*, 2167–2177. [CrossRef]

17. Zhang, Z.; Zeng, P.; Wen, Y.; He, L.; He, X. Comprehensive Assessment of BDS-2 and BDS-3 Precise Orbits Based on B1I/B3I and B1C/B2a Frequencies from iGMAS. *Remote Sens.* **2023**, *15*, 582. [CrossRef]

18. Zhang, Y.; Kubo, N.; Chen, J.; Wang, J.; Wang, H. Initial Positioning Assessment of BDS New Satellites and New Signals. *Remote Sens.* **2019**, *11*, 1320. [CrossRef]

19. Wang, E.; Yang, T.; Wang, Z.; Zhang, Y.; Guo, J.; Shu, W.; Qu, P. Performance evaluation of precise point positioning for BeiDou-3 B1c/B2a signals in the global range. *Sensors* **2021**, *21*, 5780. [CrossRef]

20. Li, X.; Li, X.; Liu, G.; Yuan, Y.; Freeshah, M.; Zhang, K.; Zhou, F. BDS multi-frequency PPP ambiguity resolution with new B2a/B2b/B2a+b signals and legacy B1I/B3I signals. *J. Geod.* **2020**, *94*, 107. [CrossRef]

21. Zhang, P.; Tu, R.; Wu, W.; Liu, J.; Wang, X.; Zhang, R. Initial accuracy and reliability of current BDS-3 precise positioning, velocity estimation, and time transfer (PVT). *Adv. Space Res.* **2019**, *65*, 1225–1234. [CrossRef]

22. Hu, J.; Li, P.; Zhang, X.; Bisnath, S.; Pan, L. Precise Point Positioning with BDS-2 and BDS-3 constellations: Ambiguity resolution and positioning comparison. *Adv. Space Res.* **2022**, *70*, 1830–1846. [CrossRef]

23. Wu, Z.; Wang, Q.; Hu, C.; Yu, Z.; Wu, W. Modeling and assessment of five-frequency BDS precise point positioning. *Satell. Navig.* **2022**, *3*, 8. [CrossRef]

24. Yu, X.; Cao, X.; Wang, J.; Ge, Y.; Shen, F. The benefit of B1C/B2a signals for BDS-3 wide-area decimeter-level and centimeter-level point positioning with observable-specific signal bias. *Measurement* **2023**, *214*, 112815. [CrossRef]

25. Montenbruck, O.; Steigenberger, P.; Prange, L.; Deng, Z.; Zhao, Q.; Perosanz, F.; Romero, I.; Noll, C.; Stürze, A.; Weber, G.; et al. The Multi-GNSS Experiment (MGEX) of the International GNSS Service (IGS): Achievements, prospects and challenges. *Adv. Space Res.* **2017**, *59*, 59,1671–1697. [CrossRef]

26. Deng, C.; Qi, S.; Li, Y.; Wang, Y.; Zou, X.; Tang, W.; Guo, C. A comparative analysis of navigation signals in BDS-2 and BDS-3 using zero-baseline experiments. *GPS Solut.* **2021**, *25*, 143. [CrossRef]

27. Prange, L.; Villiger, A.; Sidorov, D.; Schaer, S.; Beutler, G.; Dach, R.; Jäggi, A. Overview of CODE's MGEX solutionwith the focus on Galileo. *Adv. Space Res.* **2020**, *66*, 2786–2798. [CrossRef]

28. Guo, J.; Xu, X.; Zhao, Q.; Liu, J. Precise orbit determination for quad-constellation satellites at Wuhan University: Strategy, result validation, and comparison. *J. Geod.* **2015**, *90*, 143–159. [CrossRef]

29. Steigenberger, P.; Deng, Z.; Guo, J.; Prange, L.; Song, S.; Montenbruck, O. BeiDou-3 orbit and clock quality of the IGS Multi-GNSS Pilot Project. *Adv. Space Res.* **2023**, *71*, 355–368. [CrossRef]

30. Guo, J.; Wang, C.; Chen, G.; Xu, X.; Zhao, Q. BDS-3 precise orbit and clock solution at Wuhan University: Status and improvement. *J. Geod.* **2023**, *97*, 15. [CrossRef]

31. Zhang, R.; Tu, R.; Zhang, P.; Fan, L.; Han, J.; Wang, S.; Hong, J.; Lu, X. Optimization of Ground Tracking Stations for BDS-3 Satellite Orbit Determination. *Adv. Space Res.* **2021**, *68*, 4069–4087. [CrossRef]

32. Liu, J.; Ge, M. PANDA software and its preliminary result of positioning and orbit determination. *Wuhan Univ. J. Nat. Sci.* **2003**, *8*, 603–609. [CrossRef]

33. Duan, B.; Hugentobler, U.; Selmke, I.; Marz, S.; Killian, M.; Rott, M. BeiDou satellite radiation force models for precise orbit determination and geodetic applications. *IEEE Trans. Aerosp. Electron. Syst.* **2022**, *58*, 2823–2836. [CrossRef]

34. Rodriguez-Solano, C.J. Impact of the albedo modeling on GPS orbits. Master's Thesis, Technische Universität München (TUM), München, Germany, 2009.

35. CSNO. Available online: http://www.beidou.gov.cn/yw/gfgg/201912/t20191209_19613.html (accessed on 20 August 2023).

36. Boehm, J.; Niell, A.; Tregoning, P.; Schuh, H. Global mapping function (GMF): A new empirical mapping function based on numerical weather model data. *Geophys. Res. Lett.* **2006**, *33*. [CrossRef]

37. Wang, C.; Guo, J.; Zhao, Q.; Liu, J. Yaw attitude modeling for BeiDou I06 and BeiDou-3 satellites. *GPS Solut.* **2018**, *22*, 117. [CrossRef]
38. Dilssner, F.; Laufer, G.; Springer, T.; Schonemann, E.; Enderle, W. The BeiDou attitude model for continuous yawing MEO and IGSO spacecraft. *EGU*. **2018**. Available online: http://navigation-office.esa.int/attachments/32834482/1/EGU2018_Dilssner_Final.pdf (accessed on 20 August 2023).
39. Petit, G.; Luzum, B. *IERS Conventions 2010, Technical Report*; IERS Convention Center: Frankfurt, Germany, 2010. Available online: https://iers-conventions.obspm.fr/content/tn36.pdf (accessed on 20 August 2023).
40. Steigenberger, P.; Thoelert, S. Initial BDS-3 transmit power analysis (with BDS-2 gain pattern), 2020.
41. Ge, M.; Gendt, G.; Dick, G.; Zhang, F.P. Improving carrier-phase ambiguity resolution in global GPS network solutions. *J. Geod.* **2005**, *79*, 103–110. [CrossRef]
42. Ge, M.; Gendt, G.; Rothacher, M.; Shi, C.; Liu, J. Resolution of GPS carrier-phase ambiguities in Precise Point Positioning (PPP) with daily observations. *J. Geod.* **2008**, *82*, 389–399. [CrossRef]
43. Teunissen, P.J.G. A new method for fast carrier phase ambiguity estimation. In Proceedings of the IEEE Position, Location and Navigation Symposium, Las Vegas, NV, USA, 11–15 April 1994; IEEE: New York, NY, USA, 1994; pp. 562–573.